

Article

A Numerical Simulation Study on the Probable Maximum Typhoon Wave in the South China Sea

Jianjun Yi ¹, Xingnan Zhang ¹, Guoliang Zou ², Ke Zhang ^{1,3,4,*}  and Jianquan Wang ¹

¹ College of Hydrology and Water Resources, Hohai University, Nanjing 210024, China; wangjq@hhu.edu.cn (J.W.)

² Nanjing Hydraulic Research Institute, Nanjing 210029, China

³ China Meteorological Administration Hydro-Meteorology Key Laboratory, Nanjing 210024, China

⁴ Key Laboratory of Water Big Data Technology of Ministry of Water Resources, Hohai University, Nanjing 210024, China

* Correspondence: kzhang@hhu.edu.cn; Tel.: +86-25-83787112

Abstract: The South China Sea spans the tropics and subtropics. Tropical cyclones in the area are extremely active, due to the features of its marine environment, such as wide water-depth profile, complex topography and hydrology. The maximum wave heights along the coast of China are normally generated by typhoons. Especially in the context of global warming, extreme weather events have significantly increased in the recent years, leading to more frequent strong and super typhoons. With the development of resources and energy in China expanding into the deep sea, extreme waves have caused serious damage to sea projects, endangering people's lives and properties. Selecting the accurate typhoon gradient model to calculate various extreme waves, including the probable maximum tropical cyclone (PMTC) wave, is of significance for the safety of marine engineering construction and disaster prevention and mitigation. In this paper, we first proposed a wind field fusion model suitable for the South China Sea by superimposing an empirical typhoon model with the background wind field, and further verified it using the measured typhoon data. Secondly, the fused wind field was used as the input wind field of the SWAN (Simulating Waves Nearshore) model, and the wave fields of typhoons "Usagi" and "Mangosteen" were used to verify the model. The relevant parameters of PMTC were calculated using the Pearson Type III frequency fitting method, while the verified SWAN model was used to calculate the probable maximum typhoon wave, and P-III frequency analysis was carried out by direction of the extrapolated result of typhoon waves to obtain the design wave elements of each return period. Finally, a model for calculating the probable maximum typhoon wave suitable for this sea area was proposed to derive the characteristic parameters and time-histories of the probable maximum typhoon wave and the wave heights and their corresponding frequencies of various extreme waves.

Keywords: fused wind field; probable maximum tropical cyclone (PMTC); SWAN model; extreme waves



Citation: Yi, J.; Zhang, X.; Zou, G.; Zhang, K.; Wang, J. A Numerical Simulation Study on the Probable Maximum Typhoon Wave in the South China Sea. *Sustainability* **2023**, *15*, 10254. <https://doi.org/10.3390/su151310254>

Academic Editors: Jie Liang, Pingping Luo, Xuezhi Tan and Anlei Wei

Received: 8 March 2023

Revised: 27 May 2023

Accepted: 13 June 2023

Published: 28 June 2023



Copyright: © 2023 by the authors. Licensee MDPI, Basel, Switzerland. This article is an open access article distributed under the terms and conditions of the Creative Commons Attribution (CC BY) license (<https://creativecommons.org/licenses/by/4.0/>).

1. Introduction

China is located in the East Asian monsoon region on the west coast of the Pacific Ocean, and is the region of the world with the most typhoons that have the highest intensities and the most destructive power [1]. The South China Sea spans the tropics and subtropics. Therefore, tropical cyclones in this region are extremely active, due to the features of the marine environment, such as wide water-depth profile, complex topographic and hydrological conditions. Particularly in recent years, extreme weather events have increased significantly in the context of global warming [2]. As a result, strong and super typhoons are becoming more frequent in this region.

The maximum wave heights along the coast of China are generated by typhoons [3]. As the development of natural resources and energy in China is advancing towards deep seas, extreme waves have caused serious damage to marine engineering and structures.

After the Fukushima nuclear power accident in Japan, the probable maximum typhoon wave has been one of the important factors that must be considered in the marine disaster risk assessment of coastal large-scale projects in China [4]. Therefore, selecting the accurate typhoon gradient model to calculate various extreme waves, including the probable maximum typhoon wave, is of significance for the safety of marine engineering construction and disaster prevention and mitigation.

The development of theoretical and numerical studies of typhoons involves the meteorological numerical model and the typhoon sea surface wind field numerical model [5]. The typhoon is the low-pressure center, and can be calculated by the common pressure models such as the Holland (1980) model [6], Jelesnianski (1965) model [7], Myers (1954) model [8], Fujita (1952) model [9], Takahashi (1939) model [10] and Bjercknes (1921) model [11]. The wind field models generally include two types, namely the gradient wind field model and the boundary layer model. In the simulation of the typhoon wind field, the typhoon is often regarded as the result of superimposition of the circularly symmetrical wind field with a stationary center and the migrating wind field (Yan Bingyao, 1984) to reflect the asymmetry of the wind field [12].

The work efficiency of wave numerical simulation has been improved with the development of computers [13]. The common simulation methods include numerical solution of the Boussinesq equation, and various models evolved from the gentle slope equation, such as the parabolic model and the elliptical model [14]. The third type is the models based on energy spectrum equations, such as the SWAN (Simulating Waves Nearshore) wave model [15]. Several studies have examined the typhoon waves in the South China Sea using the SWAN model. Ge et al. simulated the characteristics of the direction spectrum of typhoon waves in the Beibu Gulf [16], while Liang et al. studied the influencing factors in the simulation of typhoon waves in the South China Sea [17]. Wang et al. evaluated the risk of dike flooding along the coast of Fujian [18]. The above three types of models have their own advantages and disadvantages [19], but the SWAN model is more widely used.

To cope with climatic and environmental changes and advocate the sustainable development of the earth and human beings, the world's energy is transforming to a low-carbon and non-carbonized development mode. An energy revolution with the theme of vigorously developing and utilizing renewable energy has emerged worldwide [20]. After more than ten years of rapid development of the offshore wind power industry, there are fewer and fewer areas close to the shore that are shallow, easy to build on and rich in wind. To strive for a greater development space, the development of offshore wind power has inevitably moved towards deepwater development. The Guangdong Offshore Wind Power Development Plan (2017–2030) (Revised) has planned 23 offshore wind power sites in the province, including four sites in the Yang Jiang Sea area of western Guangdong, with an installed capacity of 10 million kW. This is still a very difficult task. Due to the engineering investment and high risk, the development technology of offshore wind power is still lagging behind. The design theories and specifications mainly conform to the International Electrotechnical Commission (IEC) and European Det Norske Veritas (DNV) specifications, and lack the systematic design theories of typhoon and wave, which are suitable for the marine environmental conditions. In addition, the large-scale development of offshore wind turbines has become a new trend, which also means greater environmental wind, wave, flow and operating load, and which brings serious challenges to the design and operation of offshore wind turbine foundation and structure [21].

Studies show [22,23] that the wave field caused by a typhoon has unique spatial morphology and direction characteristics. The relative relation between the typhoon path and wind farm location determines the wave amplitude and spectrum. To calculate the force of extreme waves on ocean engineering, extreme wave values are needed. To accurately simulate the characteristics of extreme wave field induced by typhoons, an accurate typhoon gradient model is needed, and the typhoon model needs to be superimposed with the correct background wind field. Previous studies have not proposed a range for extreme waves, especially in the design of offshore wind power engineering, and have not included

the probable maximum possible typhoon wave. There is a lack of quantitative comparison of the characteristics of extreme waves.

The main objectives of this paper are to combine the characteristics of tropical cyclones occurring in the South China Sea and to propose a typhoon fusion wind field model, a model of probable maximum tropical cyclone and a model of probable maximum typhoon wave suitable for extreme wave analysis in the South China Sea, based on global climate reanalysis of wind field data. It provides a research basis for the calculation of extreme waves under tropical cyclones in the South China Sea.

2. Study Areas and Data Sources

2.1. Study Area

In April 2018, the Development and Reform Commission of Guangdong Province issued the Guangdong Offshore Wind Power Development Plan (2017–2030) (Revised). There are 23 planned offshore wind power sites in the province, including four planned sites in the Yang Jiang Sea area of western Guangdong, with an installed capacity of 10 million kW. According to the calculation, the average annual wind speed is 7.51 m/s and the average wind power density is about 394.1 W/m² over long chronology of a 100 m wheel height of the offshore wind farm project in this area. The dominant wind direction is NE and the dominant wind energy direction is ENE at the wheel height. The wind and wind energy direction are both relatively concentrated. According to the specifications [24,25], the wind energy resources are relatively rich in this area.

The South China Sea is likely to be hit by tropical cyclones all the year round [26]. Data analysis from 1949 to 2019 shows that 2333 tropical cyclones were generated in the Northwest Pacific, of which 27.3% made landfall in China. Of these, 27.5% were typhoons, 25.1% were severe tropical storms and 2.8% were super typhoons. Tropical cyclones that make landfall in China are concentrated in Guangdong, Hainan and Taiwan. Guangdong led the way, accounting for 34.6% of the landings.

According to the offshore wind power planning and the actual project schedule, the Yang Jiang Sea area in the west of Guangdong Province was selected as the study area. The nearest end of the site is 55 km and the farthest end is 82 km from the land shore. The sea area is 320 km² and the water depth is 40~50 m. The sea area is located in the monsoon area, and the wind direction and speed have an obvious seasonality. Northerly winds prevail in winter, while easterly winds dominate in spring and autumn, and southwest winds dominate in summer. The annual average wind speed is 4.7 m/s, and the maximum wind speed is 36.3 m/s. The calculation and analysis of the offshore wind waves show that these mainly occur in the direction of NE-E-ENE-ESE-SE-SSE, and the E-ESE typhoon wave height is the largest in each direction.

In order to facilitate the selection of tropical cyclones within a certain range, the location of the study center was set as 112.244° E and 20.955° N (Figure 1).

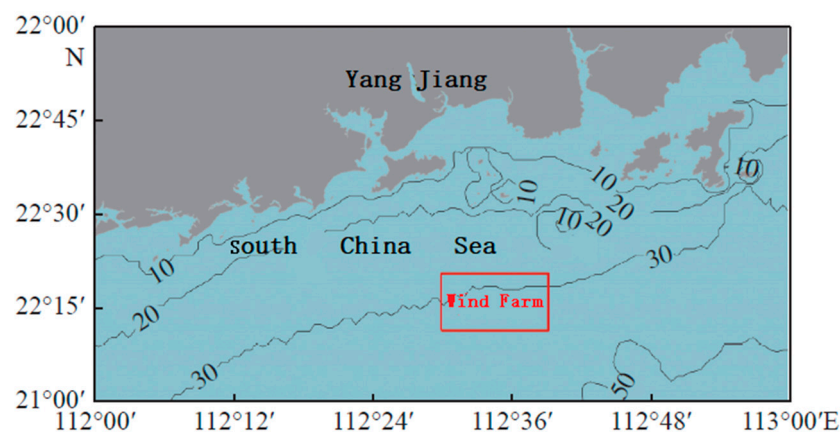


Figure 1. Map of the study area (grey lines indicate the isobath in m).

2.2. Representation of the Study Area and Data Sources

The large-scale computing grid of the typhoon wave for the study is shown in Figure 2, while Figure 3 shows the small-scale computing grid.

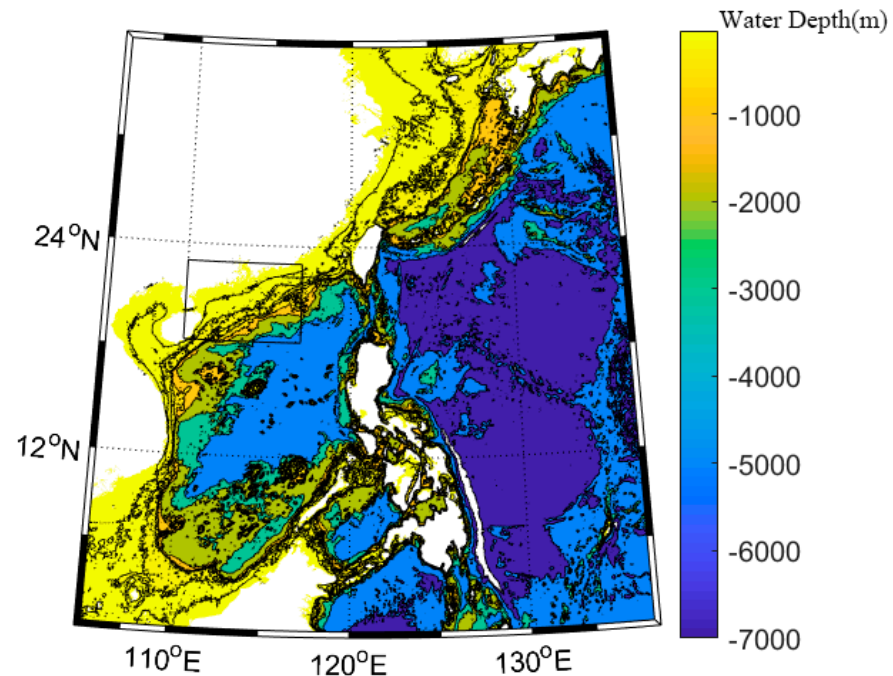


Figure 2. Large-scale computing grid of the typhoon wind and wave model; the black box is the small-range computing grid range.

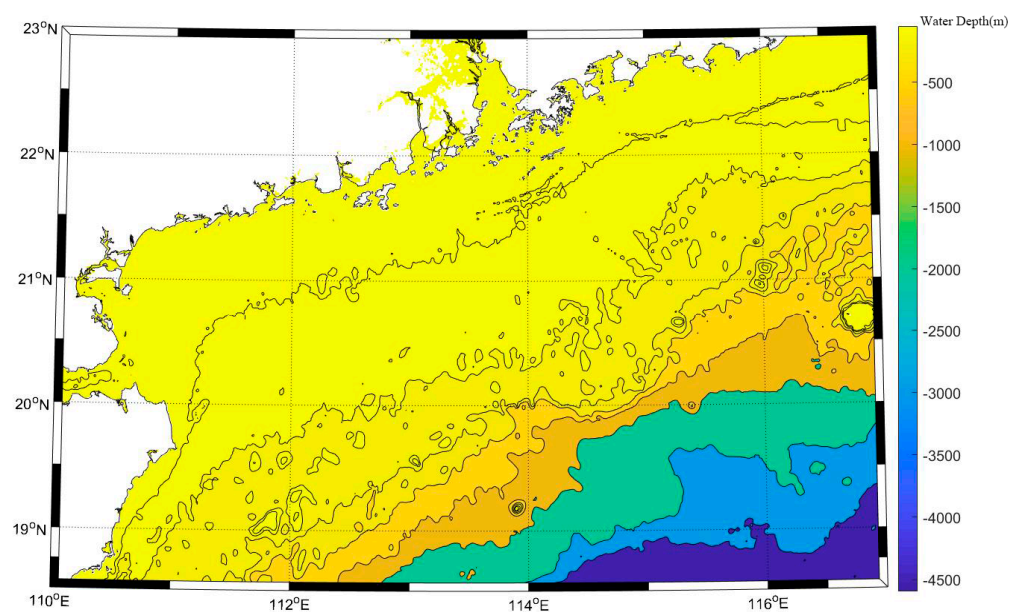


Figure 3. Small-scale computing grid of typhoon wind and wave model.

The main data and their sources used in this study are as follows. The tropical cyclone track data from 1949 to 2019 were derived from the Typhoon Yearbooks of the National Meteorological Center and the Typhoon Yearbook of the South China Sea Ocean Atlas. Short-term measured wave data and buoy observation data (QF303 and QF306) were available from 2016 to 2017. Other meteorological data include wind tower measured data of offshore wind power plant in the sea area, aircraft typhoon detection data in the Northwest Pacific, and Dongsha and Xisha wind observation data from the National

Meteorological Center typhoon network (<http://typhoon.nmc.cn/web.html> accessed on 17 October 2022). The bathymetric data used for numerical simulations in the study area were obtained from the National Oceanic and Atmospheric Administration. Topography data were derived from the ETOPO1 global data of NOAA (<https://maps.ngdc.noaa.gov/viewers/wcs-client/> accessed on 28 October 2022) [27], and the depth data within the calculated range were processed by interpolation. The background wind field data were derived from the fifth-generation global climate reanalysis data (ERA5), which is the fifth generation atmospheric reanalysis data set of the global climate from January 1950 to the present, calculated by the European Center for Medium-Range Weather Forecast (ECMWF). The time resolution of the background wind field data is 1 h, and the spatial resolution is $0.1^\circ \times 0.1^\circ$. The complete data set can be obtained from the following website: <https://cds.climate.copernicus.eu/cdsapp#!/dataset> accessed on 3 November 2022.

3. Model Description

3.1. Fusion Wind Field Model

3.1.1. Typhoon Pressure Field Model

The typhoon pressure field model is expressed with the combination of the Takahashi formula and Fujita formula, as shown in the equations below:

$$\begin{cases} P_r = (P_\infty - P_0) \left(1 - \frac{1}{\sqrt{1+2(r^2/R^2)}} \right) + P_0, & 0 \leq r < 2R \\ P_r = (P_\infty - P_0) \left(1 - \frac{1}{\sqrt{1+r/R}} \right) + P_0, & 2R \leq r < \infty \end{cases} \quad (1)$$

where R is the maximum wind speed radius of the typhoon; P_0 is the pressure at the center of the typhoon; P_∞ is the pressure outside the typhoon (normal pressure); r is the distance between a certain place in the pressure field and the center of the typhoon; and P_r is the pressure at a distance r from the center of the typhoon.

The wind field in the typhoon domain is formed by the superimposition of two vector fields. One is the centrosymmetric wind field in the typhoon domain, and the other is the moving wind field where the typhoon moves in the atmosphere as a system.

For the centrosymmetric wind field, the gradient wind formula can be used to calculate the corresponding wind field distribution, and the obtained gradient wind field can better describe the situation of the typhoon eye area. The gradient wind formula is:

$$V_g = -\frac{1}{2}f_r + \left[\left(\frac{1}{2}f \right)^2 + \frac{r}{\rho} \frac{\partial P}{\partial r} \right]^{\frac{1}{2}} \quad (2)$$

In the calculation of the moving wind field, the commonly-used formulas are the Miyazaki (1961) and Ueno Takeo (1981) formulas as follows:

$$V_d = V_{dx} \exp\left(\frac{-\pi r}{r_e}\right) \vec{i} + V_{dy} \exp\left(\frac{-\pi r}{r_e}\right) \vec{j} \quad (3)$$

$$V_d = V_{dx} \exp\left(-\frac{\pi}{4} \frac{|r-R|}{R}\right) \vec{i} + V_{dy} \exp\left(-\frac{\pi}{4} \frac{|r-R|}{R}\right) \vec{j} \quad (4)$$

where, V_{dx} and V_{dy} are the components of the typhoon's moving speed in the x and y directions; and r_e is the attenuation coefficient, which is generally taken as 500 km. The expression methods of the above two formulas are similar in the wind speed attenuation rate, but the difference is that the latter adopts the maximum wind speed radius, while the former directly gives the exponential attenuation distribution. Since the maximum wind speed radius can be easily obtained through empirical formulas, the Ueno Takeo formula (1981) is used here as the formula for calculating the moving wind field.

According to the above gradient wind formula and the Ueno Takeo formula, the typhoon wind field distribution under the Fujita–Takahashi formula can be obtained:

When $0 \leq r < 2R$,

$$U = C_1 V_{dx} \exp\left(-\frac{\pi}{4} \frac{|r-R|}{R}\right) - C_2 \left(-\frac{f}{2} + \sqrt{\frac{f^2}{4} + \frac{2\Delta P}{\rho_a R^2} \left[1 + 2\left(\frac{r}{R}\right)^2\right]^{-\frac{3}{2}}}\right) \times [(x - x_c) \sin \alpha + (y - y_c) \cos \alpha] \quad (5)$$

$$V = C_1 V_{dy} \exp\left(-\frac{\pi}{4} \frac{|r-R|}{R}\right) + C_2 \left(-\frac{f}{2} + \sqrt{\frac{f^2}{4} + \frac{2\Delta P}{\rho_a R^2} \left[1 + 2\left(\frac{r}{R}\right)^2\right]^{-\frac{3}{2}}}\right) \times [(x - x_c) \cos \alpha + (y - y_c) \sin \alpha] \quad (6)$$

When $2R \leq r < \infty$,

$$U = C_1 V_{dx} \exp\left(-\frac{\pi}{4} \frac{|r-R|}{R}\right) - C_2 \left[-\frac{f}{2} + \sqrt{\frac{f^2}{4} + \frac{\Delta P}{\rho_a R r} \left[1 + \frac{r}{R}\right]^{-2}}\right] \times [(x - x_c) \sin \alpha + (y - y_c) \cos \alpha] \quad (7)$$

$$V = C_1 V_{dy} \exp\left(-\frac{\pi}{4} \frac{|r-R|}{R}\right) + C_2 \left[-\frac{f}{2} + \sqrt{\frac{f^2}{4} + \frac{\Delta P}{\rho_a R r} \left[1 + \frac{r}{R}\right]^{-2}}\right] \times [(x - x_c) \cos \alpha - (y - y_c) \sin \alpha] \quad (8)$$

where, $\Delta P = P_\infty - P_0$; x_c and y_c are respectively the center positions of the tropical storm (m); $r = \sqrt{(x - x_c)^2 + (y - y_c)^2}$ is the distance from any point in the wind area to the center of the tropical storm; U and V are the actual wind speed at any point in the wind area; ρ_a (kg/m^3) is the standard atmospheric density; C_1 and C_2 are empirical constants, which are taken as 1.0 and 0.8 respectively; and α is the inflow angle, taken as 20° ; f is the Coriolis force parameter.

3.1.2. Fusion of the Background Wind Field

Appendini et al. calculated and analyzed NCEP, ERA-I and JRA-25 reanalysis data in 2012 and found that the ERA wind field was more suitable for extreme weather modeling and analysis [28].

The wind field of the typhoon model and the background wind field (ERA5) were fused as follows:

$$\begin{cases} V_c = V_M & r < R_1 \\ V_c = (1 - \alpha)V_M + \alpha V_Q & R_1 \leq r \leq R_2 \\ V_c = V_Q & r > R_2 \end{cases} \quad (9)$$

where, V_M is the empirical model wind field; V_Q is the background wind field; and α is the weight coefficient, which ensures the smooth connection of the two wind fields. R_1 , R_2 and α are adjusted accordingly in the simulation.

The ERA5 data have a spatial resolution of about 30 km and have 137 vertical layers from the surface to an altitude of 80 km to parse the atmosphere, including uncertainty information for all variables at reduced spatial and temporal resolutions of 1 h and $0.1^\circ \times 0.1^\circ$.

3.1.3. Wind Field Verification

In order to test the accuracy of the fusion wind field, the measured wind speed data were selected for verification. The simulation accuracy of the fusion wind field was tested by a root mean square error and a correlation coefficient.

$$RMSE = \sqrt{\frac{1}{N} \sum_{i=1}^N (V_m(i) - V_0(i))^2} \quad (10)$$

$$CORREL = \frac{\frac{1}{N} \sum_{i=1}^N [V_m(i) - \overline{V_m}] \cdot [V_0(i) - \overline{V_0}]}{\left\{ \frac{1}{N} \sum_{i=1}^N [V_m(i) - \overline{V_m}]^2 \right\}^{\frac{1}{2}} \cdot \left\{ \frac{1}{N} \sum_{i=1}^N [V_0(i) - \overline{V_0}]^2 \right\}^{\frac{1}{2}}} \quad (11)$$

$$\overline{V_m} = \frac{1}{N} \sum_{i=1}^N V_m(i) \quad (12)$$

$$\overline{V_0} = \frac{1}{N} \sum_{i=1}^N V_0(i) \quad (13)$$

where $V_0(i)$ is the observed sample value; and $V_m(i)$ is the calculated values for the model.

Typhoon 0110-YUTU was a typhoon generated in the western Pacific Ocean, which entered into the South China Sea (from 06:00 on 23 July 2001 to 12:00 on 26 July 2001). The accuracy statistics are shown in Table 1. Figures 4 and 5 show the comparison of the values of the wind field fusion model and the observed values during the typhoon period at Dongsha ($20^{\circ}40' N$, $116^{\circ}43' E$) and Xisha ($16^{\circ}50' N$, $112^{\circ}20' E$) stations, respectively. It can be seen that the fusion wind field is relatively close to the measured maximum wind speed, and the correlation coefficient is high. Therefore, the fusion wind field proposed in this paper can reasonably describe the typhoon process in the study area.

Table 1. Accuracy statistics of structural wind field and measured value during Typhoon YUTU.

Statistics	Dongsha Station ($20^{\circ}40' N$, $116^{\circ}43' E$)		Xisha Station ($16^{\circ}50' N$, $112^{\circ}20' E$)	
	Typhoon Field	Fusion Wind Field	Typhoon Field	Fusion Wind Field
RMSE	1.9756	0.8940	0.8875	0.5421
CORREL	0.95159	0.99114	0.92181	0.97688

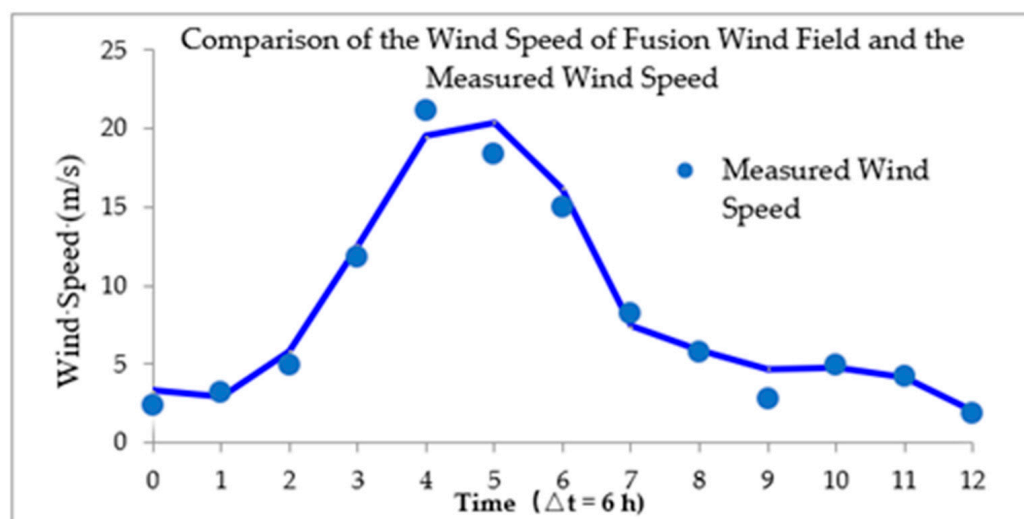


Figure 4. Comparison between the fusion wind speed and the observed wind speed at Dongsha station ($20^{\circ}40' N$, $116^{\circ}43' E$) during the time course of Typhoon YUTU.

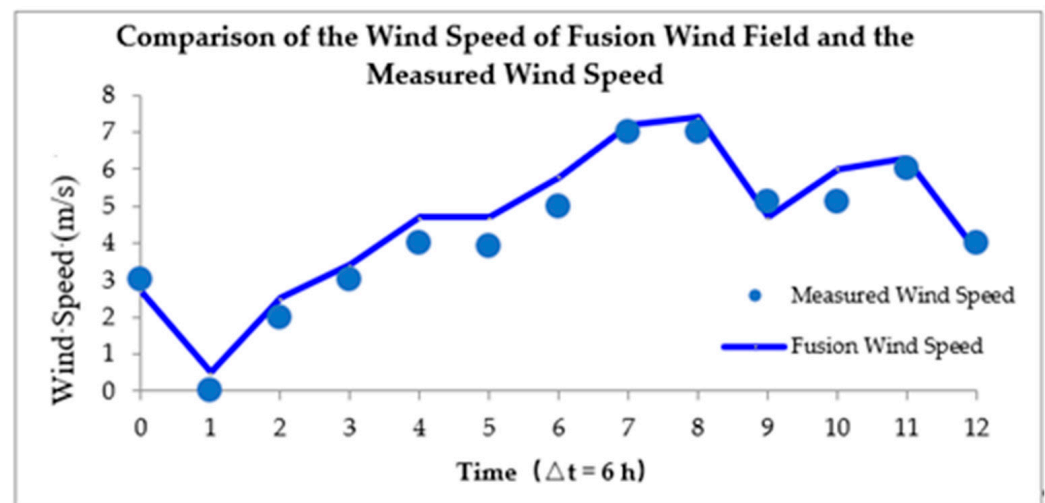


Figure 5. Comparison between the fusion wind speed and the observed wind speed at Xisha station (16°50' N, 112°20' E) during Typhoon YUTU.

3.2. SWAN Wave Model

3.2.1. Delineation and Determination of SWAN

The third-generation sea wave numerical calculation model SWAN is developed and maintained by the Civil Engineering Department of the Netherlands University of Technology. The SWAN model is powerful and can be used to calculate wind-generated surface gravity waves at any scale.

The SWAN model adopts the dynamic spectrum balance equation as the governing equation to describe ocean waves. The governing equation in the Cartesian coordinate system is:

$$\frac{\partial}{\partial t}N + \frac{\partial}{\partial x}C_xN + \frac{\partial}{\partial y}C_yN + \frac{\partial}{\partial \sigma}C_\sigma N + \frac{\partial}{\partial \theta}C_\theta N = \frac{S}{\sigma} \quad (14)$$

The first term on the left side of the equation stands for the rate of change of the dynamic spectral density in time, the second and third terms for the propagation of the dynamic spectral density in geometric space, the fourth term for the frequency shift caused by current and water depth changes, and the fifth term for the refraction and shallowing effects caused by current and water depth changes. The S on the right side of the equation stands for the energy source sink items, including the wind energy input item, whitecap dissipation, bottom friction, dissipation caused by shallowing and breaking, four-wave interaction and three-wave interaction. C_x , C_y , C_σ and C_θ stand for the propagation speeds of the dynamic spectral density in the x , y , σ and θ spaces, respectively.

$$C_x = \frac{dx}{dt} = \frac{1}{2} \left[1 + \frac{2kd}{\sinh(2kd)} \right] \frac{\sigma k_x}{k^2} + U_x \quad (15)$$

$$C_y = \frac{dy}{dt} = \frac{1}{2} \left[1 + \frac{2kd}{\sinh(2kd)} \right] \frac{\sigma k_y}{k^2} + U_y \quad (16)$$

$$C_\sigma = \frac{d\sigma}{dt} = \frac{\partial \sigma}{\partial d} \left[\frac{\partial d}{\partial t} + \vec{U} \cdot \nabla d \right] - C_g \vec{k} \cdot \frac{\partial \vec{U}}{\partial S} \quad (17)$$

$$C_\theta = \frac{d\theta}{dt} = \frac{1}{k} \left[\frac{\partial \sigma}{\partial d} \frac{\partial d}{\partial m} + \vec{k} \cdot \frac{\partial \vec{U}}{\partial m} \right] \quad (18)$$

The energy action of the SWAN model is mainly considered in five aspects:

$$S = S_{in} + S_{nl} + S_{ds} + S_{bot} + S_{surf} \quad (19)$$

where S_{in} is wind energy input; S_{nl} is the energy transfer in nonlinear wave interactions; S_{ds} is the wavy whitecap dissipation; S_{bot} is the energy loss from bottom friction; and S_{surf} is the energy loss from breaking waves.

The mathematical models usually adopt two boundary conditions, i.e., open boundary (waterside) and closed boundary (shore). For the open boundary, the surge boundary is used for control.

$$\zeta|_b = \zeta(x, y, t) \quad (20)$$

For the closed boundary, according to the principle of inaccessibility, the wave boundary is taken as 0, namely

$$\zeta|_b = 0 \quad (21)$$

At the beginning of the calculation, the wave action at each point in the entire calculation area is the initial condition of the calculation, namely

$$\zeta(x, y, t_0) = \zeta_0(x, y) \quad (22)$$

3.2.2. Verification of the Typhoon Wave Model

In this study, the mesh accuracy of large-range is 0.1° , and the mesh of small-range is $1/40^\circ$. In the calculation, the default JONSWAP spectrum was adopted. This was centered on the local main wave direction/wind direction and distributed in accordance with the direction. The frequency and direction segmentation parameters adopted the values recommended by the SWAN user manual, which were suitable for the typhoon wave calculation. The frequency calculation ranged from 0.04 to 1.0, the direction segmentation was 36, and the resolution was 10° . Consider five energy actions according to Equation (19).

The locations of the wave observation points are shown in Figure 6. The location of QF306 was 112.37° E, 21.07° N, while the location of QF303 was 115.59° E, 22.28° N (Figure 3). The model was verified using Typhoon “Usagi” in 2013 (i.e., Typhoon 1319-Usagi) and Typhoon “Mangosteen” in 2018 (i.e., Typhoon 1822-Mangosteen).

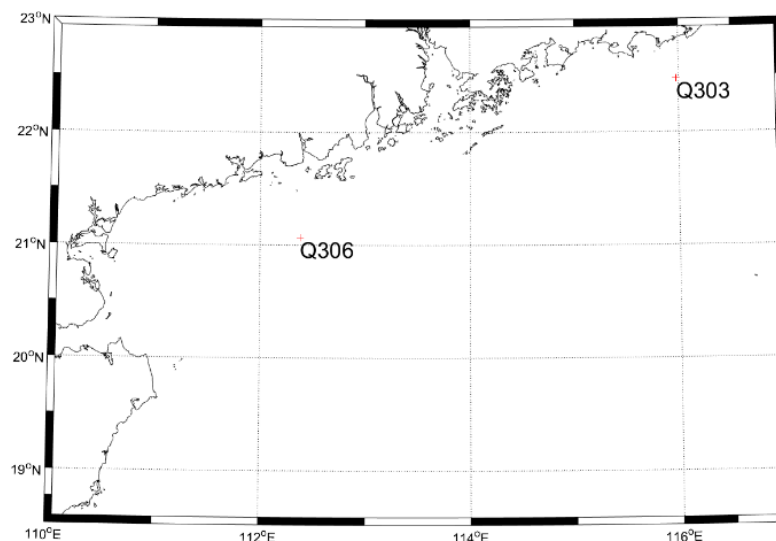


Figure 6. Locations of the observation points.

Typhoon 1319-Usagi was formed in the Northwest Pacific Ocean, east of the Philippines, at 2 a.m. on 17 September 2013. The Hong Kong Observatory upgraded Usagi to a severe typhoon at 12:45 a.m. On 20 September, Usagi took a west-northwest path and accelerated to 18 km/h, with its intensity reaching its peak in the morning. It made landfall on the southern coast of Shanwei City, Guangdong Province, China with a maximum wind force 14 (45 m/s) near the landfall center. The maximum sustained wind speed in the center reached 162 km/h. After landfall, the wind continued to move northwest and

entered Guangxi at noon on 23 September. The wind speed continued to weaken, and then the National Meteorological Center stopped its numbering; its moving path is shown in Figure 7. Figure 8 shows the comparison between the model calculation results and the observed significant wave height of Buoy QF303.

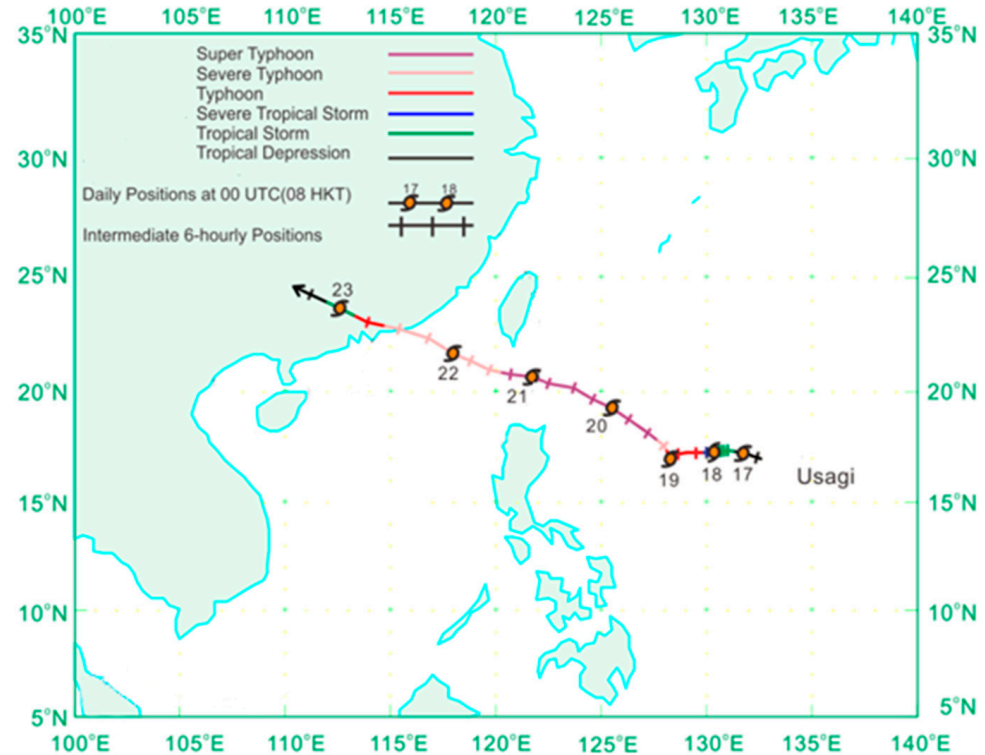


Figure 7. Moving path of Typhoon No. 19-Usagi in 2013.

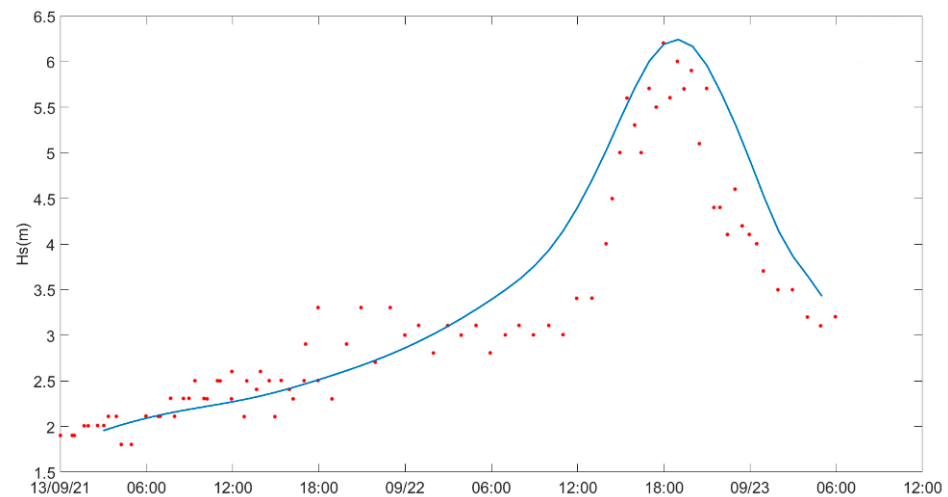


Figure 8. Verification of significant wave height of Buoy QF303 during Typhoon Usagi in 2013; points are the observed values, while the line is the pattern value.

Typhoon 1822-Mangkhut was generated on 4 September 2018 in the waters west of the International Date Line, and was upgraded to a super typhoon on 11 September. It landed in the northern Philippines at 1:40 a.m. on 15 September and moved towards the South China Sea at a speed of 25 km per hour. At 17:00 on 16 September, it made landfall in Haiyan Town, Taishan, Guangdong Province, China. At landfall, the lowest central pressure was 955 pha and the maximum nearby wind force was level 14 (45 m/s, equivalent to 162 km/h). Typhoon Mangkhut had a huge cloud system, a wind circle radius of 350 km

to 600 km and a diameter range of 1000 km. Figure 9 shows the moving path of Typhoon 1822-Mangkhut. Figure 10 shows the comparison between the model calculation results and the observed significant wave height of Buoy QF306.

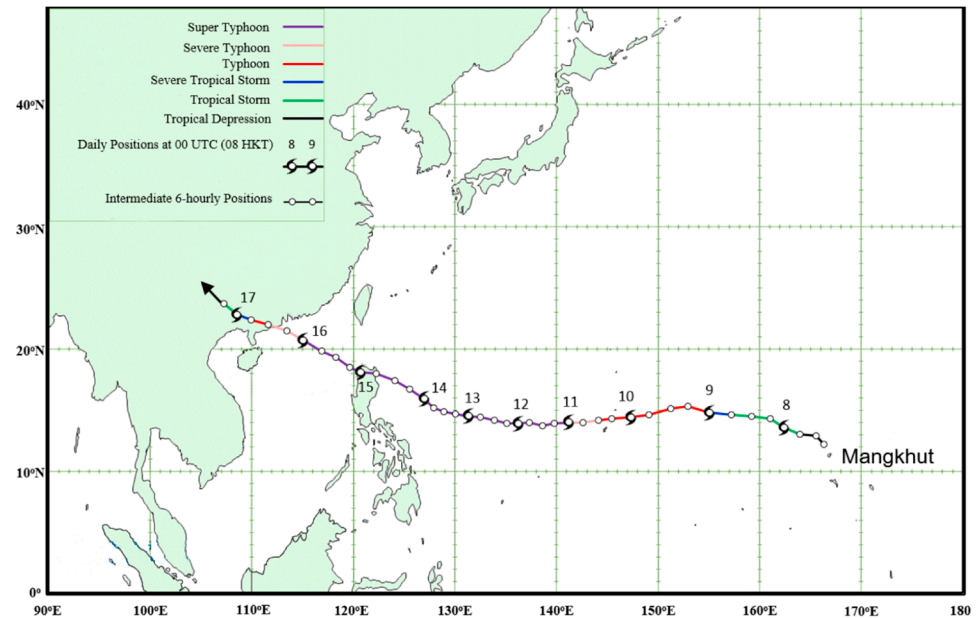


Figure 9. Moving path of Typhoon No. 22-Mangkhut in 2018.

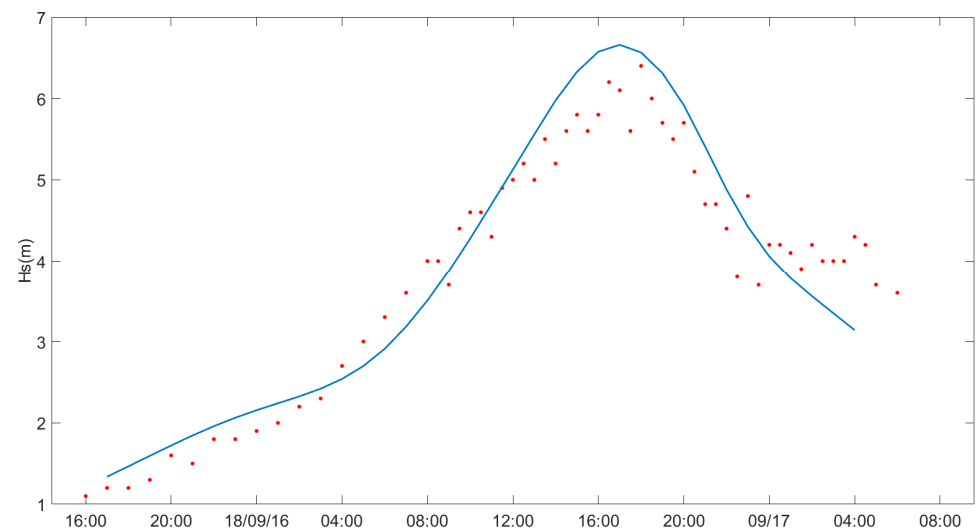


Figure 10. Verification of significant wave height of Buoy QF306 during Typhoon Mangkhut in 2018; points are the observed values, while the line is the pattern value.

The results show that the wave height calculated by using the fusion wind field model combined with SWAN was in good agreement with the actual measurement.

4. Results and Discussion

4.1. Calculation of the Probable Maximum Typhoon Wave

The probable maximum typhoon wave is generated by the probable maximum tropical cyclone (PMTTC). The PMTTC is a hypothetical steady-state tropical cyclone, which is a combination of meteorological parameter values selected according to the maximum sustained wind speed that can occur in a specific sea area (or near the coast). From these meteorological parameter values, it is possible to derive the probable maximum tropical cyclone.

Various parameters need to be taken for the calculation, so the reference location must be selected, as shown in Section 2.1. Figure 11 shows the typhoon moving paths in the study area.

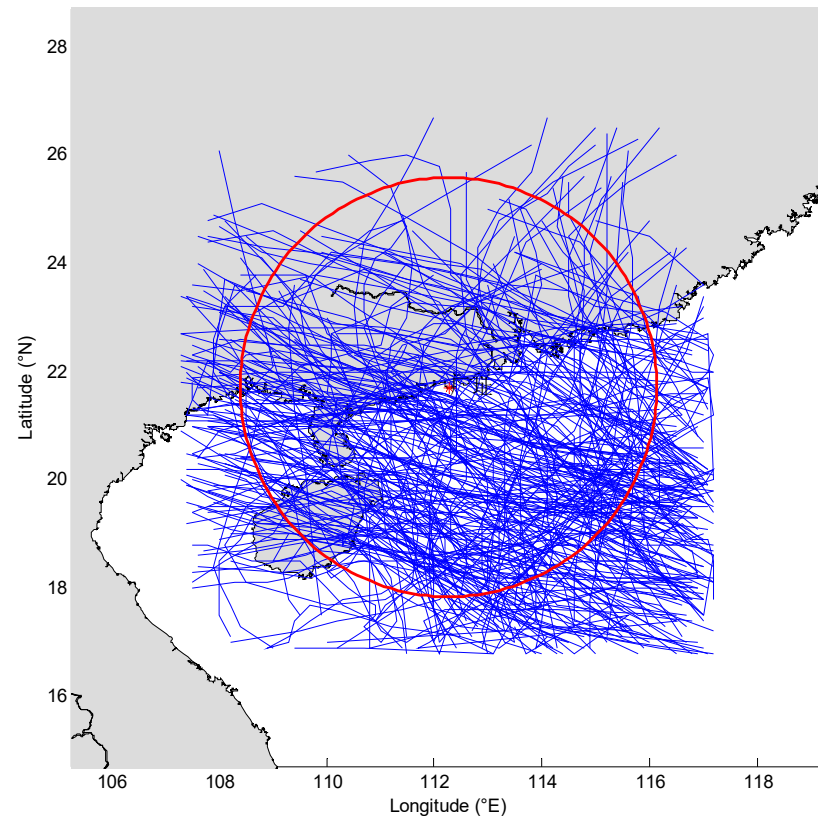


Figure 11. Typhoon path diagram (Blue solid line—typhoon track, red solid line circle is the study area (red plus sign) as the center radius of the range of 400 km).

The relevant parameters for calculating PMTC with the statistical method are described in the following sections.

4.1.1. Typhoon Outer Pressure

Typhoon outer pressure (P_{∞}) stands for the peripheral pressure or normal pressure of the typhoon, which can select the average of the annual, seasonal, monthly, and subsequent pressures at the sea level in the attack area. In this study, the statistical average of the typhoon season (April to November) in Shanwei, Shangchuan Island and Zhanjiang stations along the coast of South China was selected, and 1008 hPa was used as the peripheral pressure of PMTC, which is equivalent to the multi-year average pressure during the typhoon season along the coast of South China. The typhoon wind speed was proportional to the difference between P_{∞} and the typhoon center pressure (P_0).

4.1.2. Calculation of P_0 with the Probability Theory Method

Using 71 years' data, from 1949 to 2019, released by the China Meteorological Administration, the annual minimum pressure of the typhoon center within 400 km of the South China Sea Research Center was selected as a statistical sample. The samples of the lowest central pressure in typhoon are shown in Appendix A. If no typhoon entered the area or the typhoon had weakened to a low pressure in a certain year, the lowest pressure of the year was taken as 990 hPa. The P_0 calculated with the P-III type method (as shown in Figure 12) under the once-in-a-millennium return period was 884 hPa.

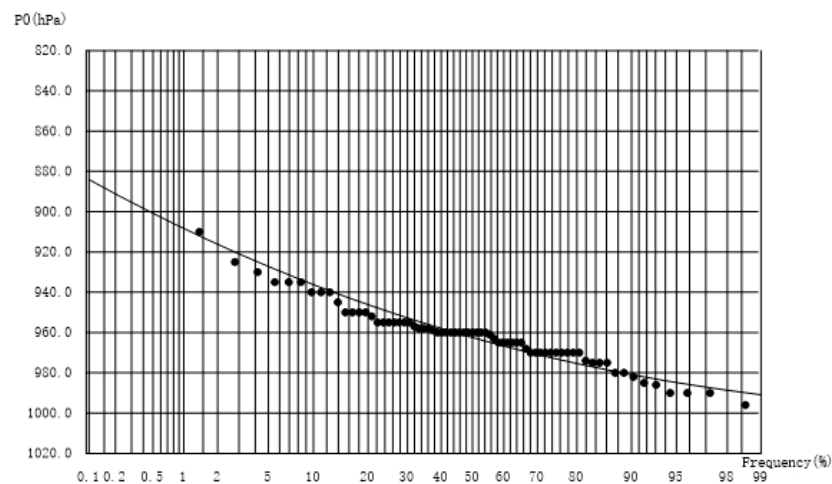


Figure 12. Fitted return period of typhoon central pressure P_0 (P-III Type) (black dots are statistical samples).

4.1.3. Maximum Wind Speed Radius of the Typhoon

According to the aircraft detection results of the maximum wind speed radius in the Northwest Pacific Ocean and the Atlantic Ocean, when P_0 is 884 hPa, the recommended typhoon maximum wind speed radius is 30 km.

4.1.4. Typhoon Moving Speed

For typhoons with the central pressure less than 975 hPa, the typhoon's positions at two time levels within the range of 400 km at a water depth of -60 m were analyzed, as shown in Table 2. As can be seen from the table, the typhoon's moving direction and speed were obtained, and the moving wind speed in the W~NW direction was between 10~40 km/h.

Table 2. Typhoon moving speed statistical table of three azimuth moving speed.

Direction	Max Moving Speed (km/h)	Range of Velocity (km/h)
W	39.8	10~40
WNW	37.7	10~38
NW	30.0	10~30

4.1.5. Typhoon Paths

The path of the typhoons that had the greatest impact in the study area were W-NW, as shown in Figure 13. The paths of the probable maximum typhoon waves can be classified into three types, namely WW, which passes through Taiwan Island and the Philippine Islands; WNW and NW; see Figure 14.

4.2. Analysis of the Probable Maximum Typhoon Wave Results

Under the once-in-a-thousand-year return period, the typhoon central pressure P_0 , P_∞ , and maximum wind radius were set as 884.0 hPa, 1008 hPa, and 30 km, respectively. According to Table 2, typhoon movement in three directions was finally selected as the typhoon movement in calculating the probable maximum typhoon wave. Within the range of movement speed in each direction (from average movement speed to maximum movement speed), 2 km/h was set as the interval. Multiple paths with each velocity (distance from the center of the study area was 3 R, 2.5 R, 2 R, 1.5 R, R and 0.5 R) were the typhoon parameters calculated for the probable maximum typhoon wave.

The calculation was carried out using the above typhoon parameters and paths, with the SWAN model, and the results show that, due to the impact of the ENE~WSW isobaths, the height of the W-directed typhoon wave in the deepwater area had a certain weakening.

The probable maximum typhoon wave in the study area was generated by a NW-directed typhoon with a moving speed of 30 km/h.

The calculated wave height and cycle results were as follows: the maximum significant wave height at -60 m in the study area was 16.5 m, and the average cycle was 16.2 s; the maximum significant wave height at -70 m was 17.1 m, and the average cycle was 16.3 s.

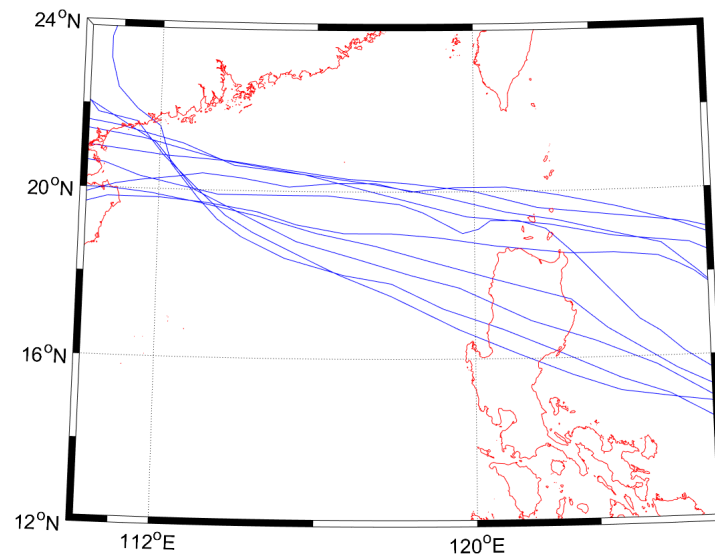


Figure 13. Moving path of the typhoons with greatest impacts on the study area (Solid blue line—Typhoon track. Solid red line—coastline).

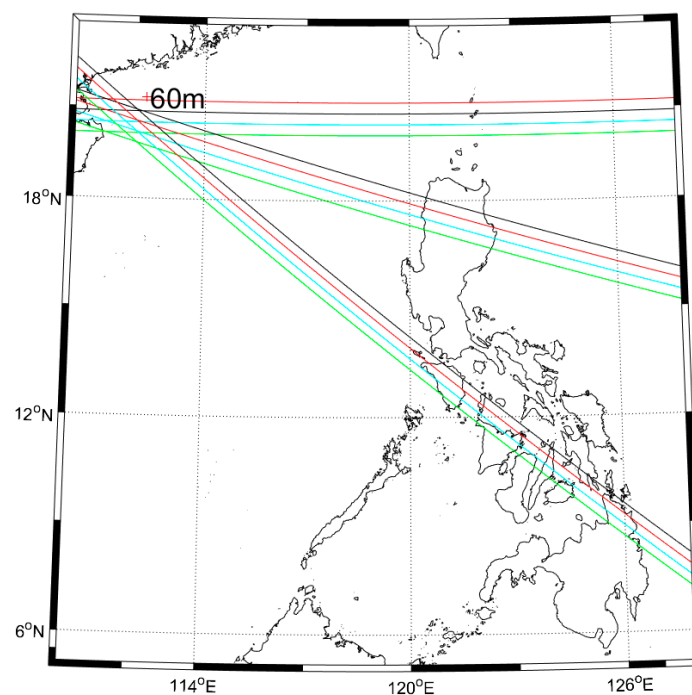


Figure 14. Moving paths of the probable maximum typhoon waves (Red plus—the center of the study area, solid black line—the coastline, solid lines in other colors represent the apparent typhoon path).

4.3. Actual Maximum Typhoon Wave

In 1954, Typhoon 5413 was formed in the Pacific Ocean, east of the Philippines, on 24 August, and landed in the coastal area from Zhanjiang to Haikang in Guangdong Province on 30 August. The central pressure at the time of landing was 950 hPa, the maximum wind speed near the center was 45 m/s, and the wind force was more than 12.

When the typhoon passed near the study area, the central pressure was 930~940 hPa, and the maximum wind speed was 50~55 m/s, which is equivalent to the typhoon under the once-in-50-year return period at a water depth of -50 m.

Typhoon 5413 in this area was calculated by using the wave mathematical model established and verified in this paper. The typhoon caused waves with a maximum significant wave height of 12.01 m at a water depth of -50 m in the study area. The distribution of significant wave height during Typhoon 5413 is shown in Figure 15, the change of wind speed is in Figure 16, the change of wave height is in Figure 17, and the time history of wind and waves is in Figure 18. It can be seen that the maximum wind speed of 45.3 m/s is equivalent to a typhoon under the once-in-50-year return period. During the typhoon period, the duration of time in which the wind speed in the study area was over 40 m/s was 4 h, and the duration of time in which the significant wave height was over 11 m was 3 h.

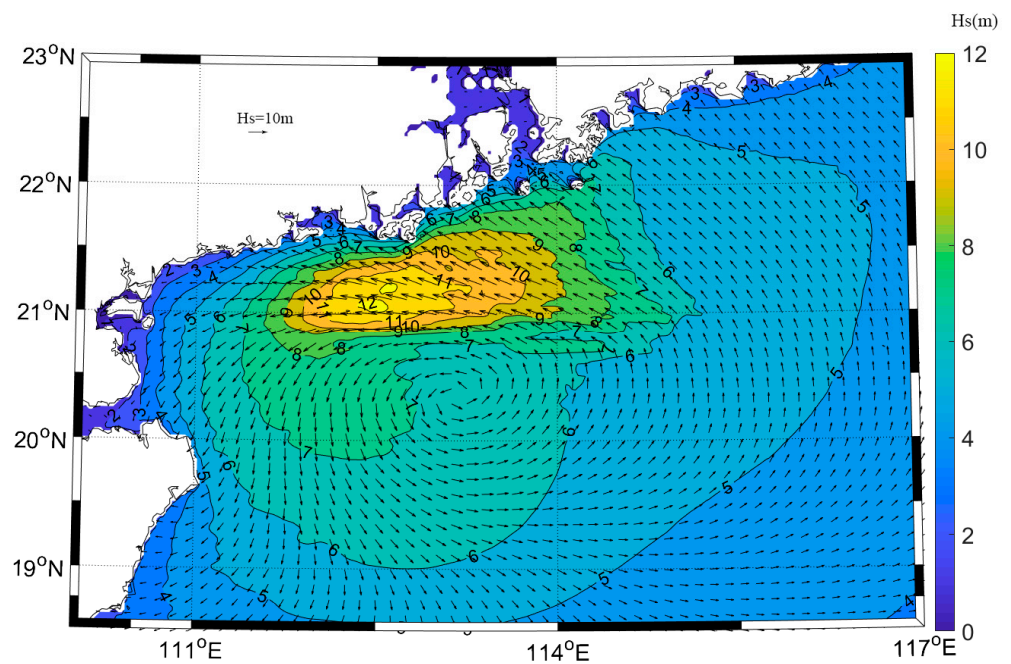


Figure 15. Distribution of significant wave height in the study area during Typhoon 13 in 1954.

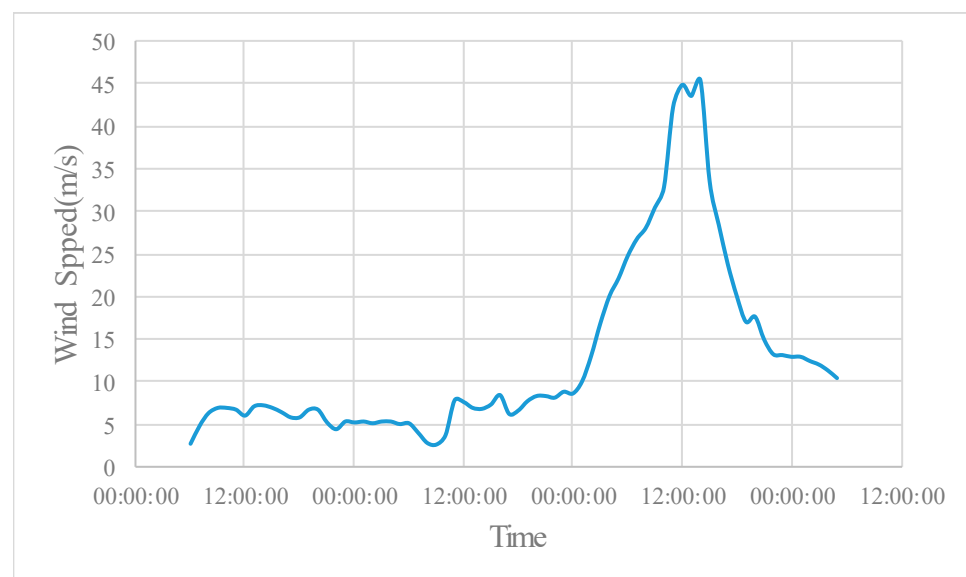


Figure 16. Variation of wind speed in the study area during Typhoon 13 in 1954.

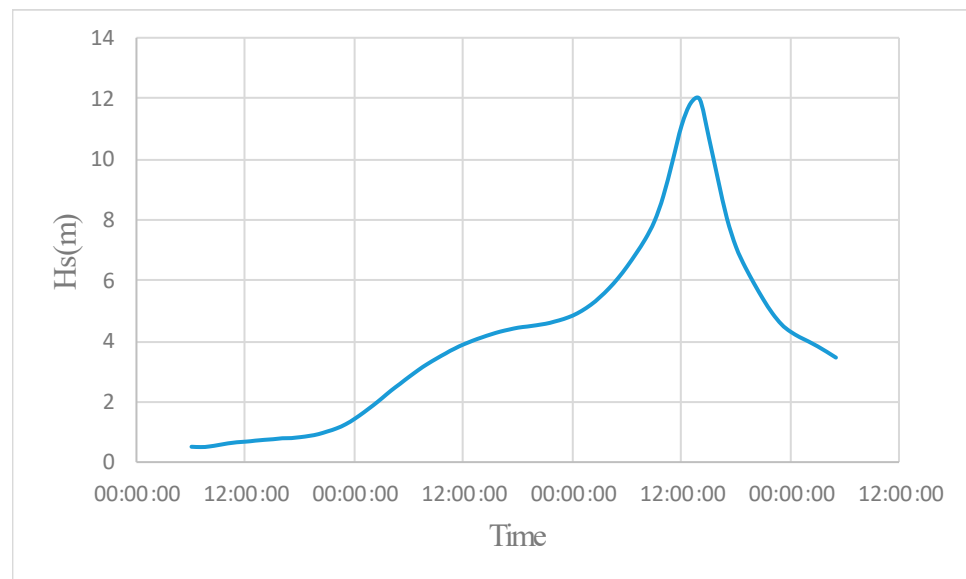


Figure 17. Wave height variation in the study area during Typhoon 13 in 1953.

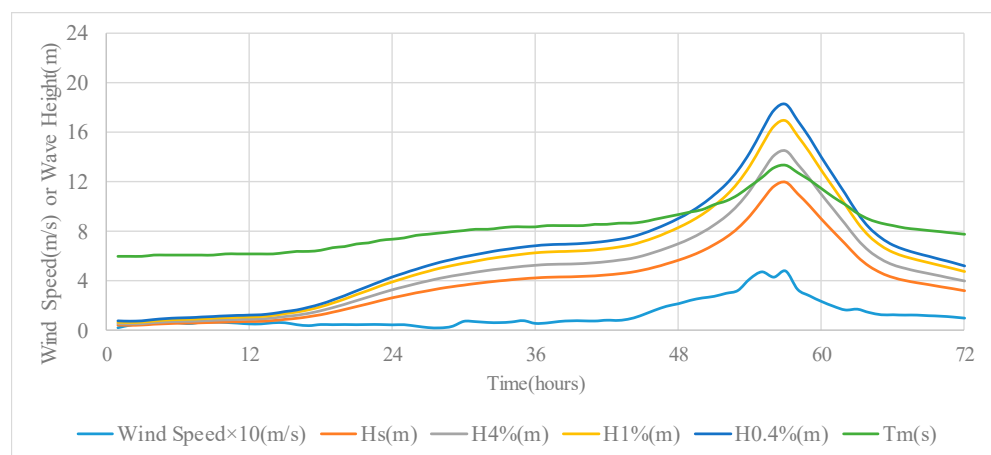


Figure 18. Time courses of wind and waves generated by the strongest Typhoon 5413 in the study area.

4.4. Discussion

The comparison of various extreme waves is shown in Table 3 and Figure 19. The results show that the trend of wave height and period is consistent under different return periods. The higher the return period is, the larger the wave height and period are. In the same recurrence period, the wave height and period are slightly larger at the depth of 10 m. The height and period of a 1000-year design wave are slightly larger than the probable maximum typhoon wave. The once-in-50 year return period design wave, its wave height and period, are equivalent to the actual maximum typhoon wave in this sea area. The actual maximum typhoon wave in this sea area is equivalent to the once-in-50-year return period, and the time history analysis can be used in engineering design practice.

Wave load is the main load borne by the structure of an offshore platform, which is closely related to wave height, water depth, wavelength, etc. The force of extreme waves on ocean engineering is generated by extreme waves. Due to different geographical locations, composition of sea and land and atmospheric and circulation regimes between countries in the world, different wave calculation models and design characteristic wave heights and return periods are used by different countries for the design of ocean engineering waves. For example, China adopts the 1% cumulative frequency wave height with a return period of 50 years in the design of offshore wind power foundations, while the USA adopts the effective wave height with a return period of 100 years. The Norwegian standard uses a

significant wave height with a return period of 50 years. The calculation model of extreme waves and the comparison of wave values proposed in this paper can provide a reference for the design of extreme wave values in different countries and regions.

Table 3. Comparison of various extreme waves ¹.

Extreme Wave	Water Depth 50 m		Water Depth 60 m		Water Depth 70 m	
	Hs (m)	T (s)	Hs (m)	T (s)	Hs (m)	T (s)
Once-in-a-millennium			17.2	16.5	17.5	16.5
Probable maximum typhoon wave			16.5	16.2	17.1	16.3
Once-in-a-hundred-year			13.2	14	13.8	14.3
Once-in-50-year			12.1	13.4	12.6	13.7
Actual typhoon wave	12.01	13.4				

¹ The actual central pressure of Typhoon 5413 at a water depth of –50 m is equivalent to a typhoon under the once-in-50-year return period.

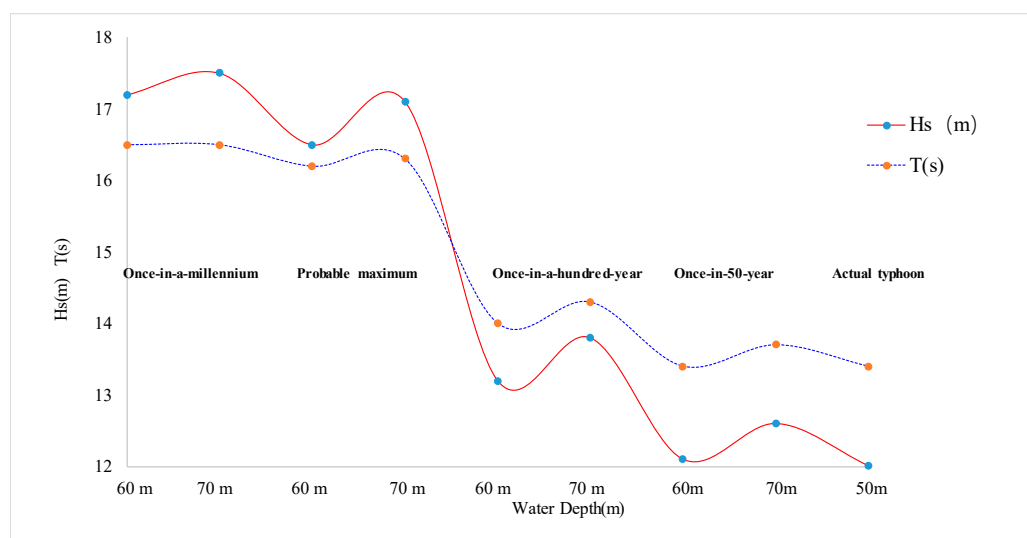


Figure 19. Comparison of various extreme waves.

5. Conclusions

Selecting the accurate wind field is the key to correctly simulating typhoon waves. In this paper, the measured typhoon was selected to verify the applicability of the gradient typhoon field fusion model in the South China Sea region. Using the Ueno Takeo typhoon model superimposed with the background wind field can obtain accurate and reliable typhoon simulation results.

According to the physical process of typhoon wave generation and development, the source-sink terms in the SWAN model were processed using the third-generation wave model SWAN, based on the typical typhoon path, The relevant parameters of PMTC were calculated with the statistical method and then, according to the actual situation in the South China Sea region, a set of applicable calculation parameters was selected to calculate the probable maximum typhoon wave. The P-III distribution was used to conduct directional frequency analysis on all typhoon wave calculation results, and the design wave elements for each return period were obtained, and wind and wave time history analysis was carried out on the actual maximum typhoon wave.

A comparison of various extreme waves shows that the design wave under the once-in-a-millennium return period is larger than the probable maximum typhoon wave and, according to the theoretical calculation, the wave under the once-in-50-year return period is equivalent to the largest typhoon wave that actually occurs in this sea area.

The model for calculating the probable maximum typhoon wave is applicable to this study area. The derived time-histories, wave heights and associated frequencies of the maximum typhoon waves corresponding to various extreme waves provide important reference values for safety, as well as disaster fortification and reduction work in marine engineering construction.

Author Contributions: Conceptualization, J.Y. and K.Z.; Methodology, K.Z.; Software, J.Y.; Formal analysis, J.Y.; Resources, J.W.; Writing—original draft, J.Y.; Writing—review & editing, J.Y., X.Z., G.Z., K.Z. and J.W.; Supervision, X.Z.; Funding acquisition, X.Z. All authors have read and agreed to the published version of the manuscript.

Funding: This study was supported by the Fundamental Research Funds for the Central Universities of China (B220203051, B220204014).

Institutional Review Board Statement: Not applicable.

Informed Consent Statement: Not applicable.

Data Availability Statement: Data are available upon request.

Conflicts of Interest: The authors declare no conflict of interest.

Appendix A

Table A1. List of samples of minimum typhoon pressure from 1949–2019.

Year	Typhoon No	Pressure (hPa)	Month	Day	Hour	Longitude (°)	Latitude (°)
1949	-	990	7	9	18	115.5	20.7
1950	-	986	10	4	18	115.7	21.3
1951	-	970	8	1	0	115.3	20.3
1952	-	960	6	12	0	112.6	20.6
1953	-	960	8	13	6	114.5	19.5
1954	-	930	8	29	0	115.3	20.5
1955	-	958	9	24	18	112.8	18.2
1956	-	974	10	23	18	114.2	19.7
1957	-	970	9	22	0	115.1	20.9
1958	-	975	9	10	18	110.8	17.6
1959	-	996	7	5	12	115.8	21.2
1960	6001	970	6	6	6	112.6	17.7
1961	6103	975	5	19	0	113.8	21.5
1962	6213	960	8	31	18	115.7	21.6
1963	6311	958	9	6	6	115.3	20.1
1964	6403	955	7	1	12	112.6	18.4
1965	6508	965	7	14	12	114.2	19.8
1966	6608	970	7	25	18	111	20
1967	6706	970	8	2	0	111.4	20.3
1968	6808	963	8	21	6	114.7	21.6
1969	6903	970	7	28	12	114.5	23.5
1970	7013	952	10	16	6	112.4	17.5
1971	7118	959	8	15	12	114.9	19.1
1972	7220	940	11	8	0	110.8	18.6
1973	7314	925	9	13	18	111.2	19.1
1974	7423	958	10	25	6	114.3	18.2
1975	7514	965	10	14	0	115.5	21.9
1976	7610	970	7	25	0	112.8	20.5
1977	7703	957	7	20	12	110.4	19.3
1978	7801	955	4	23	18	113.1	17.7
1979	7908	955	8	2	6	114.3	22.5
1980	8007	961	7	22	12	110.3	20.2

Table A1. Cont.

Year	Typhoon No	Pressure (hPa)	Month	Day	Hour	Longitude (°)	Latitude (°)
1981	8105	965	7	3	12	110.7	17.7
1982	8217	955	9	13	0	113.1	17.7
1983	8309	965	9	8	12	115	21.2
1984	8410	955	9	5	0	112.2	18.4
1985	8515	965	9	5	12	113.1	20.6
1986	8616	955	9	4	6	115.3	19.3
1987	8721	960	11	27	12	113.1	17.6
1988	8823	980	10	22	0	111.7	17.8
1989	8905	960	6	9	18	111	17.6
1990	9003	965	5	17	18	113.2	18.1
1991	9106	960	7	12	18	110.8	18.6
1992	9204	960	6	28	0	109.8	18.5
1993	9302	960	6	27	0	115.3	20
1994	9419	975	8	28	6	108.6	20.6
1995	9514	950	9	20	6	113	17.9
1996	9615	935	9	8	12	115.7	20.4
1997	9710	968	8	2	6	113.9	21.1
1998	9803	985	8	10	6	113.2	20.2
1999	9902	970	4	30	0	114.5	18.3
2000	0016	960	9	9	0	110.6	18.5
2001	0103	970	7	1	18	110.8	20.8
2002	0212	980	8	4	18	115.5	22
2003	0307	950	7	23	18	112.9	20
2004	0409	990	7	16	0	115.1	21.5
2005	0518	940	9	25	6	112.4	19
2006	0601	950	5	16	18	115.3	19.5
2007	0703	990	7	5	6	108.3	21.2
2008	0814	940	9	23	6	115.7	20.4
2009	0915	960	9	14	18	113.3	21.4
2010	1003	970	7	21	18	112	19.9
2011	1117	960	9	28	18	113.8	18.8
2012	1208	960	7	23	18	113.3	21.7
2013	1329	950	11	2	6	115.3	19.9
2014	1409	910	7	18	6	111.3	19.9
2015	1522	935	10	4	6	110.5	21.1
2016	1622	955	10	21	0	115.7	21.8
2017	1713	935	8	23	3	113.8	21.8
2018	1822	945	9	16	0	115.4	20.6
2019	1907	982	7	31	15	111.8	19.7

References

1. Wu, Z.; Jiang, C.; Deng, B.; Cao, Y. Simulation of the storm surge in the South China Sea based on the coupled sea-air model. *Chin. Sci. Bull.* **2018**, *63*, 3494–3504.
2. Huang, S.C.; Zhao, X.; Lou, H.F.; Xie, Y.L. Typhoon-generated wave height due to the super typhoon in the coastal region of Zhejiang Province. *Mar. Sci. Bull.* **2012**, *31*, 369.
3. Wang, K. Research on the Spatio-Temporal Characteristics of Disastrous Ocean Dynamics under the Influence of Typhoon and Its Effect on Hazard-Bearing Bodies. Ph.D. Thesis, Chinese Academy of Sciences, Qingdao, China, 2020.
4. Zheng, X.J. Analysis of probable maximum typhoon wave for key coastal project in the Ningde City of Fujian Province. *Trans. Oceanol. Limnol.* **2021**, *4*, 55–61.
5. Zhang, L. Numerical Simulation of Wind and Waves in the South China Sea Based on Different Typhoon Field Models. Master's Thesis, Dalian Ocean University, Dalian, China, 2015.
6. Holland, G.J. An analytic model of the wind and pressure profiles in hurricanes. *Mon. Weather. Rev.* **1980**, *108*, 1212–1218. [[CrossRef](#)]
7. Jelesnianski, C.P. A numerical calculation of storm tides induced by a tropical storm impinging on a continental shelf. *Mon. Weather. Rev.* **1965**, *93*, 343–358. [[CrossRef](#)]
8. Myers, V.A. Maximum Hurricane Winds. *Bull. Am. Meteorol. Soc.* **1957**, *38*, 227–228.
9. Fujita, T.T. Pressure distribution within typhoon. *Geophys. Mag.* **1952**, *23*, 437–451.

10. Takahashi, K. Distribution of pressure and wind in a typhoon. *J. Meteorol. Soc. Jpn.* **1939**, *17*, 417–421.
11. Bjerknæs, V. On the dynamics of the circular vortex with applications to the atmosphere and atmospheric vortex and wave motions. By V. Bjerknæs. Kristiania, Geofvsiake Publikationer, 2, No. 4, 1921. 4°. Pp. 89. Kr. 6,00. *Q. J. R. Meteorol. Soc.* **1922**, *48*, 375–376. [CrossRef]
12. Yan, L.Y. Typhoon Gradient Wind Field Model. *Mar. Forecast. Serv.* **1984**, *1*, 12–17.
13. Ji, H.D.; Lin, Y.H.; Lan, Y.Y.; Tu, Z.S.; Xiao, Z. Research on Application of SWAN Model in Design Wave Element Calculation. *J. Appl. Oceanogr.* **2021**, *40*, 477–484.
14. Li, M.; Jiang, D.C. A review on the study of mild-slope equation. *Mar. Sci. Bull.* **1999**, *18*, 70–92.
15. Ris, R.C.; Holthuijsen, L.H.; Booij, N. A spectral model for waves in the near shore zone. *Coast. Eng.* **1994**, *1*, 6–7.
16. Ge, Y.J.; Zhong, Z.; Li, J. Influences of discretization scheme in spectral space on the simulation of typhoon-generated waves with SWAN. *Mar. Sci. Bull.* **2008**, *27*, 1–8.
17. Liang, S.X.; Sun, Z.C.; Yin, H.Q.; Niu, H.Y. Influence factors of typhoon wave forecast in the South Sea by SWAN model. *Adv. Mar. Sci.* **2015**, *33*, 19–30.
18. Wang, K.; Hou, Y.J.; Feng, X.R.; Li, S.Q.; Fu, C.F. Risk assessment of overtopping seawall under waves and surges for Fujian coast: A case study of typhoon usage. *Oceanol. Limnol. Sin.* **2020**, *51*, 51–58.
19. Ji, H.D.; Lan, Y.Y.; Zhao, D.B. Combined application of SWAN wave model and mild-slope equation model in the numerical simulation of waves for 0903 typhoon Lotus. *J. Appl. Oceanogr.* **2013**, *32*, 108–116.
20. Xin, J. A Practice Report on Translation of Key Factors for the Successful Development of Offshore Wind in Emerging Markets (Excerpts). Ph.D. Thesis, Dongbei University of Finance and Economics, Shenyang, China, 2012.
21. Wang, L.Z.; Hong, Y.; Gao, Y.Y.; Huang, M.F.; Guo, Z.; Lai, Y.Q.; Zhu, R.H.; Yang, Q.M.; He, B. Dynamic Catastrophe and Control of Offshore Wind Power Structures in Typhoon Environment. *Chin. J. Theor. Appl. Mech.* **2023**, *51*, 51–58.
22. Young, I. A review of the sea state generated by hurricanes. *Mar. Struct.* **2003**, *16*, 201–218. [CrossRef]
23. Nair, M.A.; Kumar, V.S.; George, V. Evolution of wave spectra during sea breeze and tropical cyclone. *Ocean. Eng.* **2021**, *219*, 108341. [CrossRef]
24. GB/T 18710-2002; Methodology of Wind Energy Resource Assessment for Wind Farm. China Communications Press: Beijing, China, 2002.
25. Wang, A.M. Typhoon Wave Assimilation Model Establishment and South China Sea Typhoon Wave Characteristics under the Background of Winter Monsoon. Ph.D. Thesis, University of Chinese Academy of Sciences, Peking, China, 2013.
26. NB/T 31147-2018; Technical Code for Wind Energy Resource Measurement and Assessment of Wind Power Projects. National Energy Administration: Beijing, China, 2018.
27. National Oceanic and Atmospheric Administration. ETOPO1 [DB/OL]. (7 January 2018). Available online: <https://maps.ngdc.noaa.gov/viewers/wcs-client> (accessed on 28 October 2022).
28. Appendini, C.M.; Torres-Freyermuth, A.; Oropeza, F.; Salles, P. *Gulf of Mexico and Caribbean Wave Hindcast: Climatology and Wind Reanalysis Assessment*; Instituto De Ingenieria Unam: Mexico City, Mexico, 2011.

Disclaimer/Publisher's Note: The statements, opinions and data contained in all publications are solely those of the individual author(s) and contributor(s) and not of MDPI and/or the editor(s). MDPI and/or the editor(s) disclaim responsibility for any injury to people or property resulting from any ideas, methods, instructions or products referred to in the content.